POLITECNICO DI TORINO
Repository ISTITUZIONALE

Analysis of laminated beams via Unified Formulation and Legendre polynomial expansions

(Article begins on next page)

23 April 2024

Analysis of laminated beams via Unified Formulation and Legendre polynomial expansions

A. Pagani,[*] A.G. de Miguel,[†] M. Petrolo,[‡] E. Carrera[§]

Department of Mechanical and Aerospace Engineering, Politecnico di Torino,
Corso Duca degli Abruzzi 24, 10129 Torino, Italy.

Author for correspondence:
E. Carrera, Professor of Aerospace Structures and Aeroelasticity,
Department of Mechanical and Aerospace Engineering,
Politecnico di Torino,
Corso Duca degli Abruzzi 24,
10129 Torino, Italy,
tel: +39 011 090 6836,
fax: +39 011 090 6899,
e-mail: erasmo.carrera@polito.it

---

[*]Research Assistant, e-mail: alfonso.pagani@polito.it
[†]Marie Curie PhD Student, e-mail: alberto.garcia@polito.it
[‡]Research Assistant, e-mail: marco.petrolo@polito.it
[§]Professor of Aerospace Structures and Aeroelasticity, e-mail: erasmo.carrera@polito.it

Abstract

A novel one-dimensional refined model for the analysis of laminated structures is presented in this paper. The Layer Wise approach in conjunction with the Carrera Unified Formulation (CUF) enables to create hierarchical refined models which are capable of detecting both local and global mechanical behaviours. In the framework of the CUF, the FEM matrices are obtained in the form of fundamental nuclei, which are independent of the theory adopted for the model and the FEM discretization along the beam axis. A hierarchical set of expansions above the cross-section is developed by adopting Legendre-class polynomials for the definition of the beam theory kinematics. In this way, the polynomial order of the expansion can be introduced as a free-parameter, enabling to vary the accuracy of the theory of structure in a straightforward manner. Compact cross-ply laminates with different number of layers, as well as more complex composite cases like box beams have been adopted to test the Hierarchical Legendre Expansions (HLE) adapted to the Layer Wise approach. The model has been verified through published literature and also through the use of the commercial software MSC Nastran.

Keywords: Refined beam theories, Finite elements, Carrera unified formulation, Layered structures, Layer Wise approach, Hierarchical Legendre Expansions.

1   Introduction

This paper is devoted to the analysis of laminated beams by means of a novel one-dimensional refined model. Nowadays composite materials are employed in many engineering applications, having a major role in the development of new advanced structures. Indeed, in the last decade major aerospace companies have started to introduce these materials not only in secondary components, but also in primary structures within the wings and the fuselage (B787 and A350). The advantages of high-performance composites in comparison with metal alloys are well-known, amongst them: high stiffness to weight ratio, high strength to weight ratio, fatigue strength, corrosion resistance or ease of formability (see the book of Tsai [1]). The modelling techniques of composite materials have become a very useful tool to develop high-performance components for many industrial applications and they serve to get a better understanding of the behaviour of composites under different conditions, such as concentrated loads, high temperatures, delamination or fatigue. In these structures, the in-plane and shear stresses and strains of the laminate play a major role in the behaviour of the material. In this context, one-dimensional models have demonstrated to be the most suitable tool in terms of effectiveness when slender structures are considered (i.e. one dimension is much higher than the others). The classical beam theories developed by Euler [2] and then by Timoshenko [3], are not adequate for the analysis of composites since they do not correctly account for shear effects. Regarding two-dimensional theories, in which the thickness is smaller than the other two dimensions, the extension of the classical plate theory to laminated structures is represented by the Classical Lamination Theory (CLT) [4], which is based on the Love-Kirchoff hypothesis and assumes perfect bonding between layers. However, the application of CLT to composite structures is limited due to its low shear moduli in comparison with the axial moduli. The First-order Shear Deformation Theory (FSDT), based on the plate theories developed by Reissner [5] and Mindlin [6], assumes linear variation of the displacements across the thickness. Although FSDT accounts for shear deformation effects, it lacks on foreseeing correctly the higher-order shear effects, which have an important role in the behaviour of composite structures. On the other hand, 3D solid finite elements provide fairly good results in representing these effects, but the elevated computational costs required to predict correctly the effects on a laminate and the inherent limitations on the aspect ratio of the solid elements prevent in some cases its use.

In order to overcome the limitations of classical theories, many refined theories have been developed over the years for the analysis of multilayered composite structures. In the following, the attention is focused on one-dimensional theories, which represent the main topic of the present paper. However, an excellent review of the first developments in the analysis of laminated beams and plates was published by Kapania and Raciti [7, 8]. The first work focused on the shear effects and buckling, while the second on vibrations and wave propagation. Depending on the relation between the number of degrees of freedom of the mathematical model and the number of layers of the laminate, two approaches can be formally utilized in the analysis of composites:

- the Equivalent Single Layer, or ESL, in which the number of unknowns is independent of the number of layers. The main drawback of this method is that the continuity of transverse shear and normal stresses is not always assured. Reddy [9] introduced a higher-order shear deformation theory of laminated plates which provides a parabolic distribution of the transverse shear strains along the thickness. These

3

strains were null at the top and bottom surfaces. Khedeir and Reddy [10, 11] made use of this theory to carry out static, dynamic and buckling analysis of symmetric and antisymmetric cross-ply beams, accounting for classical, 1st, 2nd and 3rd order models. On the other side, Matsunaga [12] employed the method of power series of expansion of the displacement field in the depth coordinate (z). The effects of the transverse shear and normal stresses were calculated by integration of the 3D equations of equilibrium in the z direction, ensuring the continuity conditions at the interface between layers and stress boundary conditions at the top and bottom surfaces. This method was also used by the same author in [13] to analyse the natural frequencies and buckling critical loads of laminated composite beams. A higher-order mixed theory was used by Rao et al. [14] to evaluate the natural frequencies of laminated and sandwich beams by using Taylor's series of expansions for the displacement variables. Karama et al. [15] presented a multi-layered laminated model for static and dynamic analysis assuring transverse shear stress continuity at the layer's interfaces by using Ossadzow's kinematics. An analysis of bi-dimensional laminated beams based on the Proper Generalized Decomposition was carried out by Vidal et al. [16], where the displacement field is assumed as a sum of separated functions of the axial and transverse components. Another work based on the ESL approach was done by Vidal and Polito [17] on the influence of the use of the Murakamis zig-zag function in the sine model for the analysis of laminated beams.

- the Layer-Wise, or LW, in which the number of degrees of freedom (hereinafter DOFs) depends directly on the number of layers. This approach has been adopted in many studies as it aims to solve the aforementioned issues by considering the properties of each single layer separately and then by imposing the continuity of the displacements (and the transverse stresses in the case of mixed formulation) at the intra-layer interfaces. The LW method was used by Pagano [18], who treated different class of problems involving any number of layers under cylindrical bending. Recently, Shimpi and Ghugal [19] introduced a new LW trigonometric shear deformation theory for two-layered laminated beams using sinusoidal functions along the thickness coordinate for the kinematics and assuring the stress-free condition at the edges and the shear stress continuity at the layers' interfaces. Surana and Nguyen [20] presented a two-dimensional curved beam formulation applied to linear static analysis using Lagrange interpolating polynomials for the approximation in the transverse direction. The authors included the laminated material behaviour in the integration for each lamina. Another two theories based on the displacement field of LW theories were proposed by Tahani [21] for static and dynamic anaysis of laminated beams. The first one was an adaptation of the plate theories to beams, whereas the second uses a straightforward procedure similar to the one used on plate and shell theories. A layerwise shear deformation theory based on the Radial Basis Functions method and a multiquadrics discretization was introduced by Ferreira [22], who used this method to analyse laminated composite and sandwich plates. Other recent contributions on this approach can be found in [23, 24, 25, 26, 27, 28].

In the present work, a new higher-order theory has been developed and assessed in the framework of the Carrera Unified Formulation (CUF). This formulation enables to develop refined models in which the approximation type and the theory order become free parameters that are introduced as inputs of the problem. A review of the most significant beam models was recently done by Carrera et al. [29], paying a special

attention to the applications of 1D CUF models. The CUF was devised to overcome the limitations of the classical beam models by describing the kinematic field in a unified manner that will be then exploited to describe the governing equations in a hierarchical and compact way. Initially, Carrera *et al.* [30, 31] proposed CUF for two-dimensional (2D) structural and multifield problems. In their original paper the order of the theory was left as a free parameter. The extension of CUF to beam modelling was carried out by Carrera and Giunta [32], using a N-order approximation based on MacLaurin polynomial series of the displacement unknown variables above the cross-section. This class of 1D CUF models, also used in other subsequent works (see for example Carrera *et al.* [33, 34]), has been named as Taylor Expansions (TE). A new model based on Lagrange polynomials and CUF was presented by Carrera and Petrolo [35]. In that work, the enhanced capabilities of the LE (Lagrange Expansion) CUF models were discussed and particular attention was given to the capability of LE to deal with 3D-elasticity solutions of various types of structures with reduced computational costs.

Refined CUF models have been widely employed for the analysis of laminated structures by using both ESL and LW approaches. The effectiveness of ESL and LW approaches in detecting both local and global behavior of composite beams was demonstrated in [36], where TE were utilized to create ESL models and LE to obtain both ESL and LW solutions. A number of refined beam theories were obtained in [37] by adopting Taylor's polynomials, trigonometric series, hyperbolic, exponential, and zig-zag functions as expansions of the unknown displacement variables above the cross-section of thick multi-layer beams. A component-wise analysis was carried out in [38], where combinations of single fibres, related matrices and single-to-multiple layers are modelled separately, but using the same variable kinematic beam elements for each component. As a result, accurate global-local solutions and geometrically exact approximations are obtained. Furthermore, TE theories have been also used for the dynamic analysis of composite rotors in various works [39, 40, 41]. A multi-line approach for the analysis of laminated composite structures was introduced in [42]. In this work, each layer is modeled by one beam discretization along the longitudinal axis, and the continuity of the displacements at the interfaces is directed by using Lagrange multipliers. Pagani *et al.* [43] developed a method based on the use of dynamic stiffness elements for the free vibration analysis of laminated composite beams. In this study, the kinematic field is described as a truncated Taylor expansion series of the generalized unknowns, and the governing equations are obtained through the strong form of the principle of virtual displacements. A recent work devoted to the analysis of compact and thin-walled laminated beams was presented in [44]. Both ESL and LW approaches are adopted in this paper by expanding the kinematic variables with TE and LE, respectively. Filippi *et al.* [45] employed Chebyshev polynomials as expansion functions to obtain a new class of refined beam models. Static and dynamic analysis of composite beams were carried out in this work, in which the solutions calculated with the Chebyshev Expansions (CE) are compared with TE and LE, amongst others.

A new approach for the analysis of 1D high-order models is presented in the present research, which employs hierarchical Legendre-type polynomials as basis functions for the development of variable kinematic theories of structures. This class of polynomials were presented by Szabó, Düster and Rank [46], who used a Legendre-type basis to develop the p-version finite element method for one-dimensional, quadrilateral and hexahedral elements. In the present paper, Hierarchical Legendre-type Expansion (HLE) models based on these polynomials are developed in the framework of CUF to analyze composite structures. Hierarchical
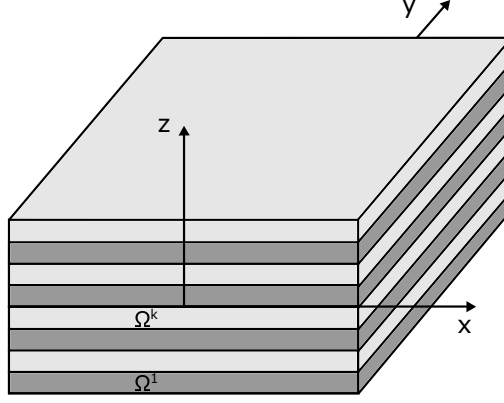
Figure 1: Reference system for a laminated beam

higher-order models can be developed thanks to the use of HLE in conjunction with the CUF, which allows us to write the governing equations and FEM arrays in a compact and general manner. The Layer-Wise approach is adopted to reproduce the laminate above the cross-section, and together with the properties of HLE models, in which the order of the expansion remains as a free-parameter that can be optimized, both local and global responses are obtained with higher levels of accuracy. The paper is structured as follows: a brief introduction of the geometrical and constitutive relations for laminated structures is given in Section 2, followed by a description of the variable kinematic models based on the CUF formulation in Section 3, with a focus on the Hierarchical Legendre model. Section 4 is dedicated to the FE application of the different CUF models and its implementation on laminates. The numerical results obtained in the different assessments considered can be found in Section 5. Finally, the conclusions of this work are in Section 6.

2 Preliminaries

Let us consider the Cartesian reference system shown in Fig. 1 for a multi-layered beam with an arbitrary number of layers. The longitudinal axis of the beam corresponds to the coordinate y ($0 \leq y \leq L$), whereas the cross-section, denoted by $\Omega = \Omega^1 \bigcup \Omega^2 \bigcup ... \bigcup \Omega^k \bigcup ... \bigcup \Omega^{N_l}$, lays on the xz-plane. Superscript k refers to the variables and parameters of each individual layer of the laminate and N_l is the total number of layers. The parameter k will be omitted in the following formulation for the sake of simplicity. The three-dimensional displacement field according to this reference system is:

$$\mathbf{u}(x, y, z) = \left\{ \begin{array}{c} u_x(x, y, z) \\ u_y(x, y, z) \\ u_z(x, y, z) \end{array} \right\} \tag{1}$$

According to classical elasticity, stress and strain tensors can be organized in six-term vectors with no lack of generality. They read, respectively:

$$\boldsymbol{\sigma}^T = \left\{ \begin{array}{cccccc} \sigma_{yy} & \sigma_{xx} & \sigma_{zz} & \sigma_{xz} & \sigma_{yz} & \sigma_{xy} \end{array} \right\}$$

$$\boldsymbol{\varepsilon}^T = \left\{ \begin{array}{cccccc} \varepsilon_{yy} & \varepsilon_{xx} & \varepsilon_{zz} & \varepsilon_{xz} & \varepsilon_{yz} & \varepsilon_{xy} \end{array} \right\} \tag{2}$$

Regarding to this expression, the geometrical relations between strains and displacements with the compact vectorial notation can be defined as:

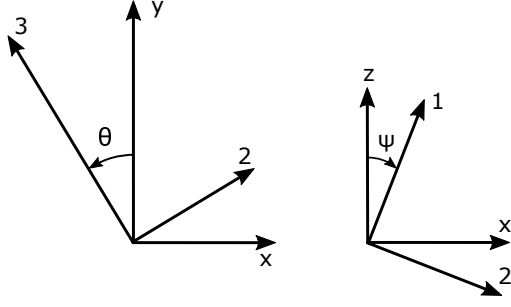$$\boldsymbol{\varepsilon} = \mathbf{D}\,\mathbf{u} \tag{3}$$

6

Figure 2: Fiber rotations

where, in the case of small deformations and angles of rotations, $\mathbf{D}$ is the following linear differential operator:

$$\mathbf{D} = \begin{bmatrix} 0 & \frac{\partial}{\partial y} & 0 \\ \frac{\partial}{\partial x} & 0 & 0 \\ 0 & 0 & \frac{\partial}{\partial z} \\ \frac{\partial}{\partial z} & 0 & \frac{\partial}{\partial x} \\ 0 & \frac{\partial}{\partial z} & \frac{\partial}{\partial y} \\ \frac{\partial}{\partial y} & \frac{\partial}{\partial x} & 0 \end{bmatrix} \tag{4}$$

In the case of fibre reinforced materials, it is well known that the mechanical properties depend on the fibre orientation angle. According to the material reference system (1,2,3) shown in 2, the Hooke's law states that:

$$\boldsymbol{\sigma_m} = \boldsymbol{C} \, \boldsymbol{\varepsilon_m} \tag{5}$$

where $\boldsymbol{C}$ is the stiffness matrix of the material, defined as:

$$\mathbf{C} = \begin{bmatrix} C_{33} & C_{23} & C_{13} & 0 & 0 & 0 \\ C_{23} & C_{22} & C_{12} & 0 & 0 & 0 \\ C_{13} & C_{12} & C_{11} & 0 & 0 & 0 \\ 0 & 0 & 0 & C_{44} & 0 & 0 \\ 0 & 0 & 0 & 0 & C_{55} & 0 \\ 0 & 0 & 0 & 0 & 0 & C_{66} \end{bmatrix} \tag{6}$$

Its coefficients C_{ij} can be found in Appendix A. In this paper, the axis 3 is parallel to the fiber orientation, whereas the axis 2 and 1 correspond to the transverse in-plane direction and the out-of-plane direction, respectively. In the global coordinate frame aforementioned (see Fig. 1), the constitutive laws become:

$$\boldsymbol{\sigma} = \tilde{\mathbf{C}} \boldsymbol{\varepsilon} \tag{7}$$

The coefficients $\tilde{C}_{ij}$ depend on the mechanical properties previously defined and on the fiber orientation angles: θ and ψ, introduced in Fig. 2. For the sake of brevity, the material coefficients in the physical coordinates are not included here, but the lector can find them in Carrera and Filippi [41].

3 Variable kinematic CUF models

Classical models (see [2] and [3]) represent the first attempts on the analysis of beams and they are dedicated to describe the mechanics of slender isotropic structures under the action of bending loads. These models neglect (EBBT) or assume a uniform shear distribution (TBT) along the cross-section, which limit its use in the modelling of composite structures. The correct analysis of multilayered beams requires the use of more

sophisticated theories in which new terms are added to the kinematic field. The Carrera Unified Formulation (CUF, see Carrera *et al.* [47]) solves this issue by describing the kinematic field in a unified manner that will be then exploited to derive the governing equations in a compact manner. The displacement field of one-dimensional models in the CUF framework is, in fact, described as a generic expansion of the primary mechanical variables through the use of arbitrary functions of the cross-section coordinates:

$$\mathbf{u}(x, y, z) = F_\tau(x, z)\mathbf{u}_\tau(y) \quad \tau = 1, 2, ..., M \tag{8}$$

where $u_\tau(y)$ is the vector of general displacements, M is the number of terms in the expansion and $F_\tau(x, z)$ defines the 1D model to be used. In fact, depending on the choice of $F_\tau(x, z)$ functions, different classes of beam theories can be implemented. Three of them are here described: TE, LE and the novel HLE.

3.1 Taylor Expansions

Taylor Expansion (TE) models make use of 2D polynomials of the type $x^i y^j$ as $F_\tau(x, z)$. For example, the third-order model, $N = 3$, leads to the following displacement field, where constant, linear, parabolic and quadratic functions are used:

$$
\begin{aligned}
u_x &= u_{x_1} + x\, u_{x_2} + z\, u_{x_3} + x^2\, u_{x_4} + xz\, u_{x_5} + z^2\, u_{x_6} + x^3\, u_{x_7} + x^2 z\, u_{x_8} + xz^2\, u_{x_9} + z^3\, u_{x_{10}} \\
u_y &= u_{y_1} + x\, u_{y_2} + z\, u_{y_3} + x^2\, u_{y_4} + xz\, u_{y_5} + z^2\, u_{y_6} + x^3\, u_{y_7} + x^2 z\, u_{y_8} + xz^2\, u_{y_9} + z^3\, u_{y_{10}} \\
u_z &= u_{z_1} + x\, u_{z_2} + z\, u_{z_3} + x^2\, u_{z_4} + xz\, u_{z_5} + z^2\, u_{z_6} + x^3\, u_{z_7} + x^2 z\, u_{z_8} + xz^2\, u_{z_9} + z^3\, u_{z_{10}}
\end{aligned} \tag{9}
$$

It is important to underline that the kinematic fields of the classical beam theories can be defined as particular cases of the first order TE model (N=1), which includes just the constant and the linear terms of Eq. (9). A more detailed description of TE models can be found in [47, 48, 29].

3.2 Lagrange Expansions

Lagrange Expansions (LE) are based on the use Lagrange polynomials as generic functions above the cross-section. The cross-section is therefore divided into a number of local expansion sub-domains, whose polynomial degree depends on the type of Lagrange expansion employed. Three-node linear L3, four-node bilinear L4, nine-node cubic L9, and sixteen-node quartic L16 polynomials can be used to formulate refined beam theories (see Carrera and Petrolo [35]). For example, the interpolation functions of a L9 expansion are defined as:

$$
\begin{aligned}
F_\tau &= \tfrac{1}{4}(r^2 + r\, r_\tau)(s^2 + s\, s_\tau) \qquad \tau = 1, 3, 5, 7 \\
F_\tau &= \tfrac{1}{2}s_\tau^2(s^2 + s\, s_\tau)(1 - r^2) + \tfrac{1}{2}r_\tau^2(r^2 + r\, r_\tau)(1 - s^2) \qquad \tau = 2, 4, 6, 8 \\
F_\tau &= (1 - r^2)(1 - s^2) \qquad \tau = 9
\end{aligned} \tag{10}
$$

where r and s vary above the cross-sectional natural plane between -1 and $+1$, and r_τ and s_τ represent the locations of the roots. The kinematic field of the single-L9 beam theory is therefore

$$
\begin{aligned}
u_x &= F_1\, u_{x_1} + F_2\, u_{x_2} + F_3\, u_{x_3} + ... + F_9\, u_{x_9} \\
u_y &= F_1\, u_{y_1} + F_2\, u_{y_2} + F_3\, u_{y_3} + ... + F_9\, u_{y_9} \\
u_z &= F_1\, u_{z_1} + F_2\, u_{z_2} + F_3\, u_{z_3} + ... + F_9\, u_{z_9}
\end{aligned} \tag{11}
$$

Refined beam models can be obtained by adopting higher order Lagrange polynomials or by using a combination of Lagrange polynomials on multi-domain cross-sections. More details about Lagrange-class models can be found in [49, 35, 48, 29].

3.3 Hierarchical Legendre Expansions

HLE (Hierarchical Legendre Expansion) models represent the object of the study of the present work. The theoretical basis of the Legendre-like functions that are adopted in this paper were presented by Szabó *et al.* [46, 50]. In those papers, the authors introduced how to use these polynomials to create sets of finite element shape functions, which will be here applied to develop hierarchical refined structural theories. The one-dimensional Legendre polynomials can be defined in several ways, being the most useful for our purposes the recurrent definition:

$$
\begin{aligned}
L_0 &= 1 \\
L_1 &= x \\
L_p &= \frac{2p-1}{p} x L_{p-1}(x) - \frac{p-1}{p} L_{p-2}(x), \quad p = 2, 3, ...
\end{aligned}
\tag{12}
$$

being p the polynomial degree. This set of polynomials represents an orthonormal basis, and their roots are identical with integration points of Gauss quadrature rules. They also satisfy the Legendre differential equation. A set of 1D functions can be defined out of this polynomials as:

$$
\tilde{L}_1(r) = \frac{1}{2}(1 - r)
\tag{13}
$$

$$
\tilde{L}_2(r) = \frac{1}{2}(1 + r)
\tag{14}
$$

$$
\tilde{L}_i(r) = \phi_{i-1}(r), \quad i = 3, 4, ..., p+1
\tag{15}
$$

where

$$
\phi_j(r) = \sqrt{\frac{2j-1}{j}} \int_{-1}^{r} L_{j-1}(x)\, dx, \quad j = 2, 3, 4, ...
\tag{16}
$$

The first two functions, i.e. Eqs.13 and 14, are the *nodal modes* and they correspond to the linear Lagrange 1D polynomials. Equation 15 includes all the *internal modes*. This Legendre-based set of functions maintains the orthogonal properties of the Legendre polynomials, in fact,

$$
\int_{-1}^{1} \frac{d\tilde{L}_i}{dr} \frac{d\tilde{L}_j}{dr}\, dx = \delta_{ij}, \quad \text{for } i \geq 3 \text{ and } j \geq 1 \text{ or } i \geq 3 \text{ and } j \geq 1
\tag{17}
$$

where δ_{ij} is the Kronecker's delta.

Two-dimensional polynomial expansions can be then defined by extending the above procedure to quadrilateral domains. In this case, nodal, edge and internal polynomials are used as interpolation functions over the domain. They are all included in Fig. 3 until the 7th order. The vertex modes are four in total, one per vertex, and they vanish at all nodes but one. Secondly, the edge modes vanish for all sides of the domain but one. Finally, the internal modes vanish at all sides, and they are just included from the fourth order expansion and higher.

Vertex expansions

The nodal or vertex modes correspond to the first-order, quadrilateral Lagrange polynomials:

$$
F_\tau = \frac{1}{4}(1 - r_\tau r)(1 - s_\tau s) \qquad \tau = 1, 2, 3, 4
\tag{18}
$$

where, as for LE models, r and s vary above the domain between -1 and $+1$, and r_τ and s_τ represent the vertex coordinates in the natural plane. In fact, the same cross-sectional functions were used to develop bilinear, LE beam theories in [35], and they were referred to as L4.
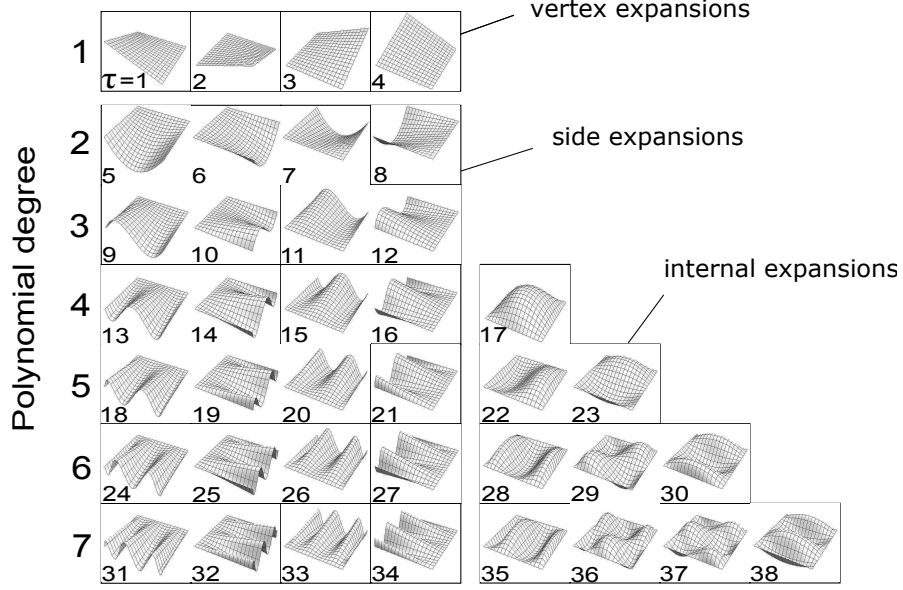
Figure 3: Hierarchical modes for quadrilaterals, including all polynomials up to the 7th order

Side expansions

The side modes are defined for $p \geq 2$ and they are defined in the natural plane as follows

$$F_\tau(r,s) = \frac{1}{2}(1-s)\phi_p(r) \qquad \tau = 5, 9, 13, 18, ... \tag{19}$$

$$F_\tau(r,s) = \frac{1}{2}(1+r)\phi_p(s) \qquad \tau = 6, 10, 14, 19, ... \tag{20}$$

$$F_\tau(r,s) = \frac{1}{2}(1+s)\phi_p(r) \qquad \tau = 7, 11, 15, 20, ... \tag{21}$$

$$F_\tau(r,s) = \frac{1}{2}(1-r)\phi_p(s) \qquad \tau = 8, 14, 16, 21, ... \tag{22}$$

where p represents the polynomial degree (see Fig. 3). It is possible to note that the above functions are expressed in such a way that they satisfy the side-continuity in multi-domain beam theories.

Internal expansions

F_τ internal expansions are built by multiplying 1D internal modes. There are $(p-2)(p-3)/2$ internal polynomials for $p \geq 4$ and they vanish at all the edges of the quadrilateral. As an example, the set of sixth-order polynomials contains 3 internal expansions (see Fig. 3), which are

$$F_{28}(r,s) = \phi_4(r)\phi_2(s) \tag{23}$$

$$F_{29}(r,s) = \phi_3(r)\phi_3(s) \tag{24}$$

$$F_{30}(r,s) = \phi_2(r)\phi_4(s) \tag{25}$$

It is important to note that the hierarchical properties of this model are related to the fact that the set of functions of a particular order contains all the polynomials of the lower degrees. As far as the sixth-order HLE model is concerned, for example, the set of functions used to define the kinematic terms of expansion includes the internal polynomials introduced in Eqs. (24), (25) and (25), and all the other internal, side and vertex functions of the same polynomial order and below, i.e $\tau = 1, ..., 30$. In fact, the variable kinematics of hierarchical CUF models define the possible deformations, shown ni Fig. 3, that the cross-section can adopt

10

as the polynomial order of the theory is increased: linear deformation for $p = 1$, quadratic for $p = 2$, cubic for $p = 3$, ..., until a required level of precision.

4   FE formulation

Various numerical methods can be developed in the framework of the CUF to solve 1D problems. The finite element formulation has been selected in the present work due to its advantages in the study of arbitrary geometries and boundary conditions. The generalized displacements are in this way described as functions of the unknown nodal vector, $\mathbf{u}_{\tau i}$, and the 1D shape functions, N_i.

$$\mathbf{u}_\tau(y) = N_i(y)\mathbf{u}_{\tau i}, \qquad i = 1, 2, ..., n_{elem} \tag{26}$$

where n_{elem} is the number of nodes per element and the unknown nodal vector is defined as

$$\mathbf{u}_{\tau i} = \left\{ \begin{array}{ccc} u_{x_{\tau i}} & u_{y_{\tau i}} & u_{z_{\tau i}} \end{array} \right\}^T \tag{27}$$

Different sets of polynomials can be used to define FEM elements. Lagrange interpolating polynomials have been chosen in this work to generate cubic one-dimensional elements. For the sake of brevity, its expressions are not included, but they can be found in the book of Carrera et.al [47], in which two-node (B2), three-node (B3) and four-node (B4) elements are described.

Finally, by introducing Eq. (8) of the cross-section expansions into the Eq. (26) of the FE discretization along the y-axis, the displacement field results:

$$\mathbf{u}(x, y, z) = F_\tau(x, z)N_i(y)\mathbf{u}_{\tau i}, \qquad \tau = 1, 2, ..., M \quad i = 1, 2, ..., n_{elem} \tag{28}$$

4.1   FEM Fundamental nucleus

The governing equations are obtained via the principle of virtual displacements. This variational statement sets as a necessary condition for the equilibrium of a structure that the virtual variation of the internal work has to be the same than the virtual variation of the external work, or:

$$\delta L_{\text{int}} = \delta L_{\text{ext}} \tag{29}$$

The internal work is equivalent to the elastic strain energy

$$\delta L_{int} = \int_l \int_\Omega \delta\boldsymbol{\varepsilon}^T \boldsymbol{\sigma} \, d\Omega \, dy \tag{30}$$

where l stands for the length of the beam and Ω is the cross-section domain. In a compact notation, the internal work can be rewritten as:

$$\delta L_{\text{int}} = \delta\mathbf{u}_{sj}^T \mathbf{K}^{\tau s i j} \mathbf{u}_{\tau i} \tag{31}$$

where $\boldsymbol{K}^{\tau s i j}$ is the fundamental nucleus of the stiffness matrix. It is important to remark that this 3×3 matrix is invariant with the order and type of structural theory. Its components, defined for the case of orthotropic
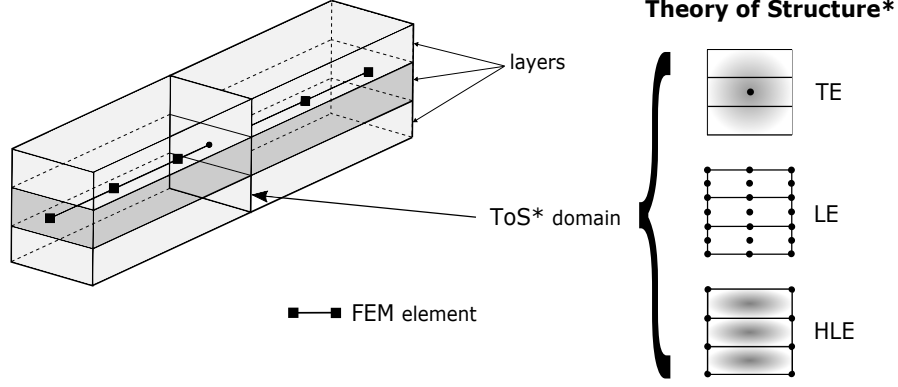
Figure 4: Differences between various refined 1D CUF finite elements

materials, are the following:

$$K_{xx}^{\tau s i j} = \widetilde{C}_{22} I_{ij} E_{\tau,x s,x} + \widetilde{C}_{44} I_{ij} E_{\tau,z s,z} + \widetilde{C}_{26} I_{ij,y} E_{\tau,x s} + \widetilde{C}_{26} I_{i,y j} E_{\tau s,x} + \widetilde{C}_{66} I_{i,y j,y} E_{\tau s}$$

$$K_{xy}^{\tau s i j} = \widetilde{C}_{23} I_{ij,y} E_{\tau,x s} + \widetilde{C}_{45} I_{ij} E_{\tau,z s,z} + \widetilde{C}_{26} I_{ij} E_{\tau,x s,x} + \widetilde{C}_{36} I_{i,y j,y} E_{\tau s} + \widetilde{C}_{66} I_{i,y j} E_{\tau s,x}$$

$$K_{xz}^{\tau s i j} = \widetilde{C}_{12} I_{ij} E_{\tau,x s,z} + \widetilde{C}_{44} I_{ij} E_{\tau,z s,x} + \widetilde{C}_{45} I_{ij,y} E_{\tau,z s} + \widetilde{C}_{16} I_{i,y j} E_{\tau s,z}$$

$$K_{yx}^{\tau s i j} = \widetilde{C}_{23} I_{i,y j} E_{\tau s,x} + \widetilde{C}_{45} I_{ij} E_{\tau,z s,z} + \widetilde{C}_{26} I_{ij} E_{\tau,x s,x} + \widetilde{C}_{36} I_{i,y j,y} E_{\tau s} + \widetilde{C}_{66} I_{ij,y} E_{\tau,x s}$$

$$K_{yy}^{\tau s i j} = \widetilde{C}_{33} I_{i,y j,y} E_{\tau s} + \widetilde{C}_{55} I_{ij} E_{\tau,z s,z} + \widetilde{C}_{36} I_{ij,y} E_{\tau,x s} + \widetilde{C}_{36} I_{i,y j} E_{\tau s,x} + \widetilde{C}_{66} I_{ij} E_{\tau,x s,x} \quad (32)$$

$$K_{yz}^{\tau s i j} = \widetilde{C}_{13} I_{i,y j} E_{\tau s,z} + \widetilde{C}_{55} I_{ij,y} E_{\tau,z s} + \widetilde{C}_{45} I_{ij} E_{\tau,z s,x} + \widetilde{C}_{16} I_{ij} E_{\tau,x s,z}$$

$$K_{zx}^{\tau s i j} = \widetilde{C}_{12} I_{ij} E_{\tau,z s,x} + \widetilde{C}_{44} I_{ij} E_{\tau,x s,z} + \widetilde{C}_{45} I_{i,y j} E_{\tau s,z} + \widetilde{C}_{16} I_{ij,y} E_{\tau,z s}$$

$$K_{zy}^{\tau s i j} = \widetilde{C}_{13} I_{ij,y} E_{\tau,z s} + \widetilde{C}_{55} I_{i,y j} E_{\tau s,z} + \widetilde{C}_{45} I_{ij} E_{\tau,x s,z} + \widetilde{C}_{16} I_{ij} E_{\tau,z s,x}$$

$$K_{zz}^{\tau s i j} = \widetilde{C}_{11} I_{ij} E_{\tau,z s,z} + \widetilde{C}_{44} I_{ij} E_{\tau,x s,x} + \widetilde{C}_{55} I_{i,y j,y} E_{\tau s} + \widetilde{C}_{45} I_{ij,y} E_{\tau,x s} + \widetilde{C}_{45} I_{i,y j} E_{\tau s,x}$$

where the E terms are the integrals of the transverse expansions above the cross-section surface and the expressions I_{ij}, $I_{ij,y}$, $I_{i,y j}$, and $I_{i,y j,y}$ refer to the integrals of the interpolation functions along y. The expressions of both kinds of integrals are included in Appendix B. The derivation of the fundamental nucleus of the loading vector from the virtual variation of the external load is not reported here for the sake of brevity, but it can be found in [47].

It should be noted that the formal expressions of the components of the fundamental nucleus of the stiffness matrix are independent on the choice of the cross-sectional functions F_τ, which determine the theory of structure, and shape functions N_i, which determine the numerical accuracy of the FEM approximation (see Fig. 4). This means that any classical to higher-order beam element can be automatically formulated by opportunely expanding the fundamental nuclei according to the indexes τ, s, i, and j.

4.2 FE application of CUF beam elements to laminated structures

In the CUF framework, the stiffness matrix of the beam elements are defined as an expansion of the fundamental nucleus. This formulation enables to create unified beam elements, which, exploding the characteristics of the fundamental nucleus, are formally independent of the order and structural theory class. The concept of the unified beam elements is illustrated in Fig. 4. The displacement unknowns that conform the kinematic field are spread over the cross-section surface by means of F_τ functions, which defined a particular theory of
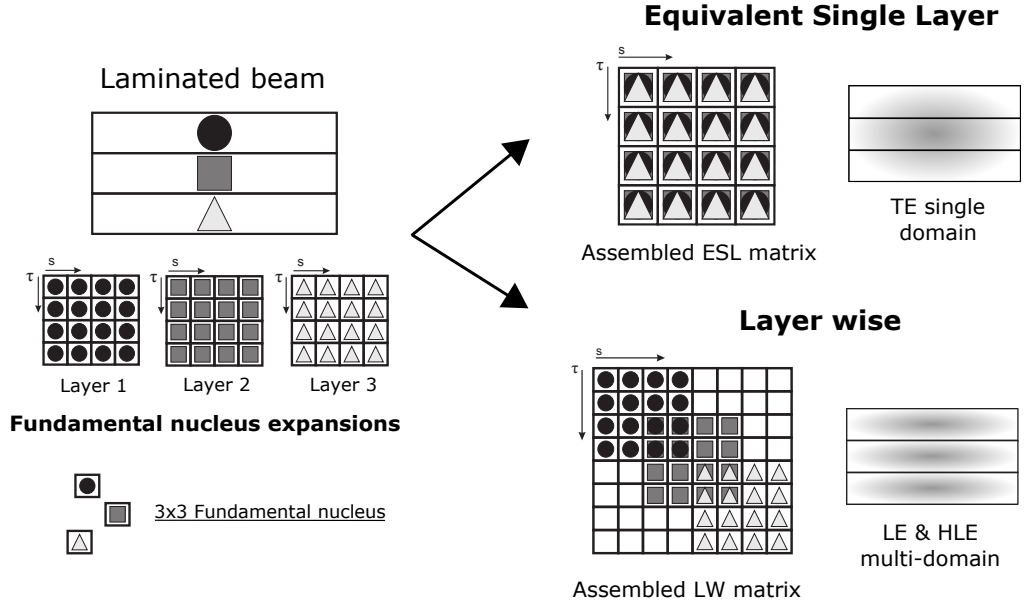
12

Figure 5: Assembly procedure of the stiffness matrix through ESL and LW approaches

structure. Since the formal expressions of the FEM arrays are the same for each class of beam theory, its choice (e.g. TE, LE or HLE) becomes independent of the type of finite element discretization used along the beam axis.

In the case of composites, the CUF provides a method to model laminates, fibers and matrices using 1D elements on the longitudinal direction and transverse expansions on the cross-section. As introduced in Section 1, two modeling approaches can be adopted for the analysis of laminated one-dimensional structures: the Equivalent Single-Layer approach, referred to as ESL, and the Layer-Wise approach, referred to as LW. Their application by means of CUF is conceptually described in Fig. 5. A brief description of each approach is provided in the following lines, extending the procedures presented in Carrera and Petrolo [36] for TE and LE to the novel HLE.

4.2.1 Equivalent Single Layer models

By using the ESL approach, the contribution of each layer of the laminate is summed when conforming the stiffness matrix, homogenizing the properties of the different layers into a single one. The result is that the multi-layer configuration is modelled as a single-layer having a set of variables assumed for the entire cross-section. ESL can be obtained through the use of any model based in CUF (e.g TE, LE and HLE). Obviously, ESL lacks in representing correctly some effects intrinsic of each layer and in their interfaces.

4.2.2 Layer-Wise models

On the other hand, LW considers separately the variables of each one of the layers. The continuity of the displacement solutions at the interfaces between layers is assured by the correspondence of the shared sides of the cross-section expansion domains. The differences between the assembly procedures for ESL and LW are shown in Fig. 5. It should be underlined that, for merely practical reasons, ESL models are obtained by means of TE in the present work, whereas LW models are obtained by employing LE and HLE. In fact, thanks to the multi-domain nature of the two latter models, LW can be implemented straightforwardly by considering
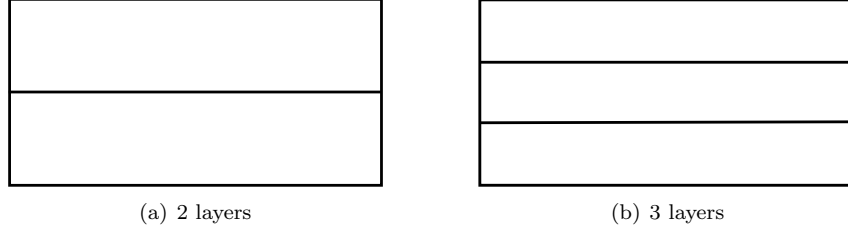
(a) 2 layers   (b) 3 layers

Figure 6: Cross-section domain configurations of the antisymmetric and symmetric laminated beams

one or several local expansions for each individual layer. Moreover, taking advantage of the aforementioned characteristics of HLE, the kinematics within the single layer can be varied hierarchically. On the other hand, in the case of LE-based LW models, the addition of mathematical layers may be necessary to improve the model capabilities to include higher-order effects. It should be added that LW can be also obtained by means of TE, but special attention must be given to the interface conditions in this case (see [51, 42]).

5 Numerical results

This section presents the results obtained from the static analysis of laminated beams through the use of one-dimensional HLE models based on CUF. Simple to complex geometries are considered in the different assessments proposed here to validate the accuracy of the present model. The first cases are related to the study of compact rectangular cross-ply beams with an increasing number of layers of the laminate, whereas the second part includes thin-walled laminated box beams under different load cases.

5.1 Antisymmetric laminated beam

A two-layer antisymmetric beam is considered first. This kind of assessment has been already discussed in various works, amongst them: Khdeir *et al.* [10], Vo and Thai [52], Pagano [53], Vidal and Polito [17] and Carrera *et al.* [37]. The dimensions of the beam are: width, $b = 0.2$ m, height, $h = 0.1$ m, and length, $L = 2$ m, being the slenderness ratio, L/b, equal to 10. According to the LW approach, LE and HLE models are developed by dividing the cross-section in two sub-domains, one per layer, as shown in Fig. 6 (a). An orthotropic material is employed for the two layers with the following properties: $E_L = 25.0$ GPa, $E_T = E_z = 1.0$ GPa, $\nu_{LT} = \nu_{Lz} = \nu_{Tz} = 0.25$, $G_{LT} = 0.5$ and $G_{Tz} = G_{Lz} = 0.2$ GPa. An antisymmetric $[0°, 90°]$ cross-ply laminate is analyzed. The beam is clamped at $y = 0$ and loaded at $y = L$ with four point forces applied at the corners of the tip cross-section. Each force has a value of 25 N and is oriented downwards in the z-direction.

The displacements and stresses are evaluated for various HLE models, including polynomial orders up to 8 (see Table 1). Seven four-node B4 elements are employed for the longitudinal discretization. A biquadratic LE model and a 3D MSC Nastran model are used as references. The displacements are evaluated at the top edge of the tip, while the stresses at the middle section of the beam. The distribution of normal and shear stresses along the z-axis at mid span are plotted in Fig. 7. Out of these results, it is possible to see that the displacements obtained through HLE models are almost the same as the one calculated with the solid model, whereas the normal and shear stress distributions coincide in great manner with the solid ones from the third polynomial order. Regarding the latter graph, the 2L9 model is not able to represent the parabolic

14

model	$-u_z \times 10^3$ m [0, L, h/2]	$\sigma_{yy} \times 10^{-3}$ [Pa] [0, L/2, h/2]	$\sigma_{yz} \times 10^{-3}$ [Pa] [0 , L/2, -h/4]	DOFs
SOLID	3.48	93.30	−11.36	132300
		LE models		
2L9	3.48	88.84	−8.18	990
		HLE models		
2HL1	3.46	90.54	−8.19	396
2HL2	3.47	88.95	−8.17	858
2HL3	3.48	89.01	−11.15	1320
2HL4	3.48	89.99	−11.15	1914
2HL5	3.48	89.11	−11.15	2640
2HL6	3.48	89.18	−11.15	3498
2HL7	3.48	89.22	−11.15	4488
2HL8	3.48	89.27	−11.15	5610

Table 1: Deflections and stresses of the antisymmetric laminated beam
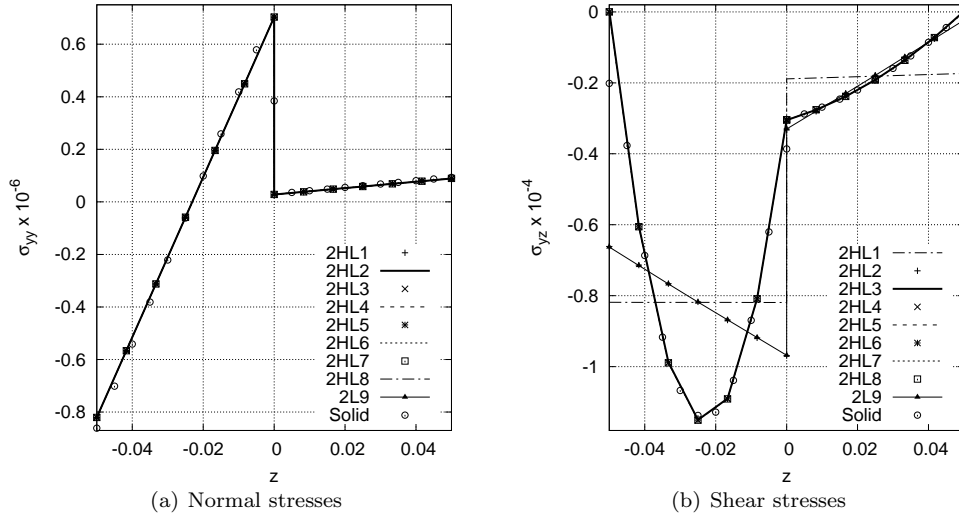

(a) Normal stresses

(b) Shear stresses

Figure 7: Normal and shear stresses along the height of the antisymmetric laminated beam at mid-span

distribution of the shear stresses along z, whereas the HLE model provides very accurate results from the third expansion order. As mentioned before, unlike HLE models, LE models do not have variable order kinematics, requiring a multi-domain description of the layers in order to obtain the correct distribution of the stress solutions.

In order to assess the quality of the FEM approximation, four discretizations of four-node B4 elements considered: 7, 14 and 21. Table 2 shows the values of displacements and stresses for a growing number of beam elements and different expansion orders. Out of this study, it is possible to see that all the solutions are in good agreement with the solid model independently of the longitudinal mesh, with the exception of the shear stresses, σ_{yz}, at the top of the cross-section. In this case, the solutions return to values close to zero as the number of FEM elements increases, satisfying the stress-free conditions at the edge. Moreover, the convergence of these solutions depend also on the polynomial order of the model, being necessary to use more beam elements as the expansion order increases. Figure 8 represents the shear stresses at the upper side of the cross-section at mid-span for an increasing number of FEM elements along y. As a consequence of these results, at least 20 FEM elements are employed in all the assessments to obtain the shear stress

model	n elements	$u_z \times 10^3$ $[0, L, h/2]$	$\sigma_{yy} \times 10^{-3}$ $[0, L/2, h/2]$	$\sigma_{yz} \times 10^{-3}$ $[0, L, -h/4]$	$\sigma_{yz} \times 10^{-3}$ $[0, L/2, h/2]$
2HL3	7	-3.48	89.01	-11.50	0.16
	14	-3.48	88.92	-11.50	0.02
	21	-3.48	88.93	-11.50	0.02
2HL5	7	-3.48	89.11	-11.51	1.44
	14	-3.48	88.83	-11.51	-0.02
	21	-3.48	88.83	-11.51	0.00
2HL8	7	-3.48	89.27	-11.51	4.14
	14	-3.48	88.92	-11.51	-0.65
	21	-3.48	88.90	-11.51	0.04

Table 2: Various solutions of displacements and stresses for different numbers of beam elements
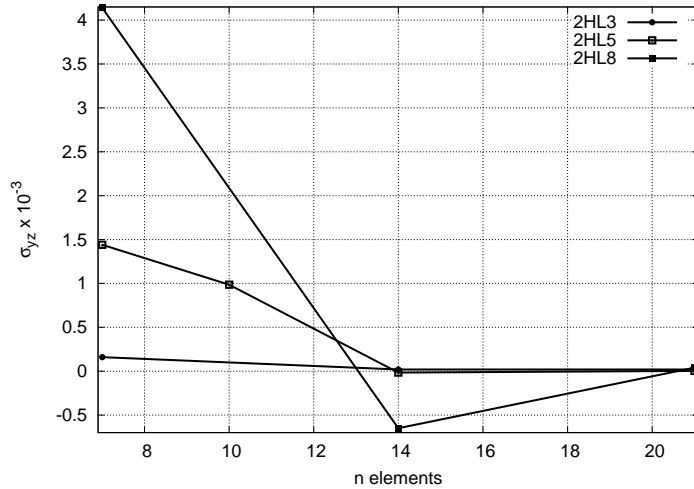

Figure 8: Shear stress at $[0, L/2, h/2]$ for different FEM discretizations

distributions, whereas the tabled results are in all cases calculated with the minimum number of B4 elements used in the literature, which is indicated for each model. It should be added that this mathematical issue, that typically occurs in equispaced interpolation points, has been already studied and different procedures have been proposed to mitigate its effects. It could be minimized, for instance, by calculating the solutions at the Chebyshev interpolation points, as it was done by Kulikov and Plotnikova [54], for which the oscillation is minimum.

5.2 Symmetric laminated beam

The same geometry as in the previous case is considered again for a tree-layer symmetric laminate. Material, loads and boundary conditions remain also unaltered. The cross-section domain division for LE and HLE models is shown in Fig. 6 (b). Table 3 displays the HLE solutions of displacements, normal stresses and shear stresses at different points of the beam. A 3L9 model and and the solid solutions obtained with the commercial code MSC Nastran are also included. The normal and shear stresses distributions along z at the mid span section are plotted in Fig. 9 for all the models considered. It is possible to see how the 3HL2 and the 3L9 models provide nearly the same linear-shape distribution. Moreover, HLE models are able to capture the parabolic distribution of the shear stresses from the 3rd expansion order (3HL3). It should be noted that, unlike the LE model, the HLE solutions satisfy the intra-laminar shear stress continuity at the interfaces of

model	$-u_z \times 10^3$ m [0, L, h/2]	$\sigma_{yy} \times 10^{-3}$ [Pa] [0, L/2, h/2]	$\sigma_{yz} \times 10^{-3}$ [Pa] [0, L/2, 0]	DOFs
SOLID	0.72	311.07	−6.92	195300
		LE models		
3L9	0.72	296.24	−6.91	1386
		HLE models		
3HL1	0.71	296.46	−6.93	528
3HL2	0.72	296.17	−6.91	1188
3HL3	0.72	296.28	−6.91	1848
3HL4	0.72	296.31	−6.92	2706
3HL5	0.72	296.34	−6.94	3762
3HL6	0.72	296.41	−6.94	5016
3HL7	0.72	296.58	−6.90	6468
3HL8	0.72	296.74	−6.90	8118

Table 3: Deflections and stresses of the symmetric laminated beam
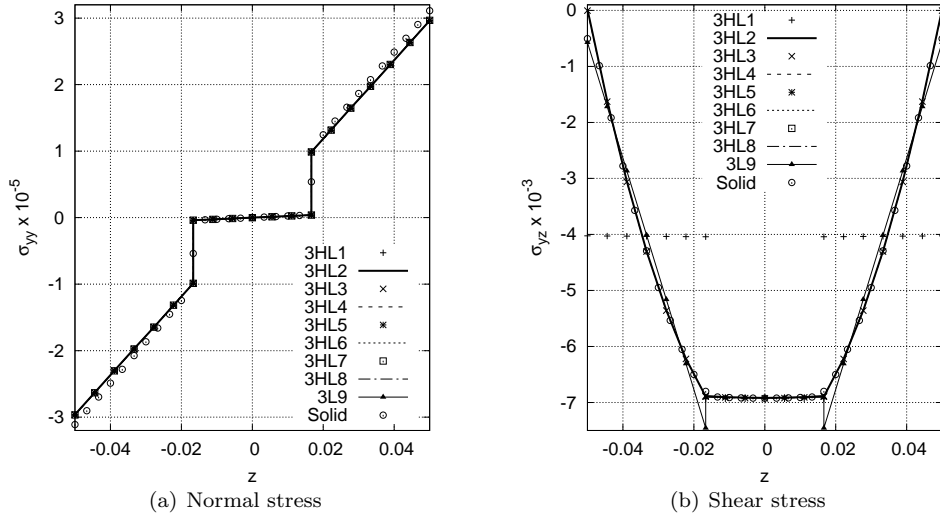

(a) Normal stress

(b) Shear stress

Figure 9: Normal and shear stress distribution along the z-axis at mid-span for the symmetric beam

the layers. This can be observed for all polynomial orders but the first (3HL1), whose linear F_τ expansions provide an almost constant distribution of the shear stresses.

5.3 Eight-layer composite beam

For the third test of the HLE on laminates, a thick eight layer cantilever beam is considered. The beam is 90 mm long and its rectangular cross-section is 10 mm high and 1 mm wide. Figure 10 shows the vertical distribution of the layers. A single-domain per layer is used to obtain Layer Wise model based on HLE and LE. Two different materials are employed for the lamination, labelled 1 and 2. Both have the same elastic modulus in the transversal direction (E_T), equal to 1 GPa, shear modulus (G_{TL}), equal to 0.5 GPa, and poisson ratio (ν), equal to 0.25. They differ in the longitudinal elastic modulus, which is 30 GPa for material 1 and 5 GPa for material 2. The poisson ratio and the shear modulus are assumed to be constant in all directions. Four equal loads are applied at the corners of the beam's tip, summing a total of −0.2 N in the vertical direction.

Displacements and stresses are again compared with other solutions of the same case found in the literature
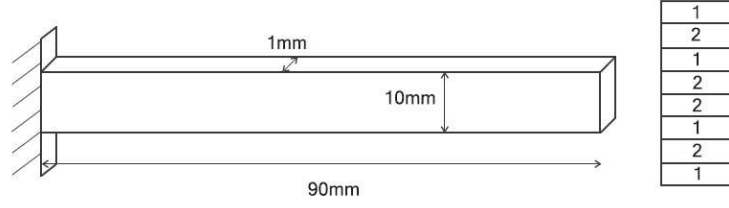
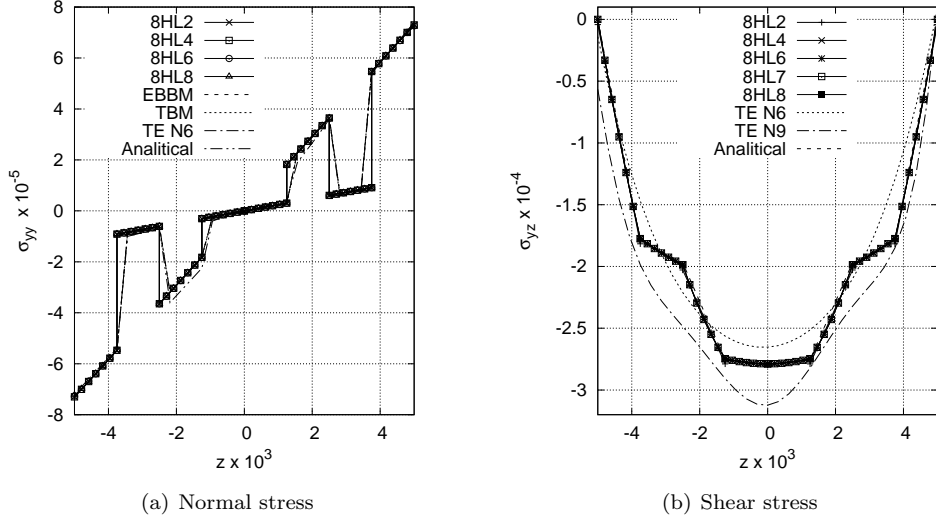Figure 10: Representation of the eight-layer beam and the lamination sequence

(a) Normal stress

(b) Shear stress

Figure 11: Normal and shear stress distribution along the z-axis at mid-span for the eight-layer composite beam

(Surana and Nguyen [20], Davalos and KimBarbero [55], Xiaoshan Lin [56], Vo and Thai [52] and Carrera *et al.* [37]). The results are displayed both in numerical and graphical form. Table 4 shows the maximum deflections and the normal stresses, σ_{yy}, at the mid span for all the models considered. CBT stands for Classical beam theory and FOBT stands for First-order beam theory. TE models and zig-zag functions expansions based on CUF are also used as reference results. The theories which contain the zig-zag term are identified with zz. Layer-wise solutions based on LE ([44]) and a Multi-Line (ML) model ([42]) are also included here. The latter model was implemented by employing 8 beam-lines (one per layer), being the two central layers modeled with a $N = 2$ TE and the rest with a $N = 3$ TE. The Figure 11 (a) displays the normal stress distributions along the z-axis at mid-span, whereas Fig. 11 (b) shows the shear stresses along the same axis. The analytical solutions, calculated according to the equations of Lekhniskii [57], are also shown in both graphs. The maximum defections reach higher values with the HLE models than with all the other models considered as references, increasing with the polynomial order. On the other hand, it is possible to state that the stress distributions obtained with the HLE models overcome the results calculated through the TE models, being almost equal to the analytical solutions previously mentioned.

5.4 Single-cell box beam

After assessing the results of HLE models on compact rectangular beam cases against other theories of structure, as well as analytical and solid solutions, it is possible to step forward to the analysis of thin-walled

model		$-u_z \times 10^5$ m	$-\sigma_{yy} \times 10^2$	$DOFs$
Surana and Nguyen [20]		3.031	720	
Davalos and KimBarbero [55]		3.060	750	
Xiaoshan Lin [56]		3.031	720	
Vo and Thai [52]		3.024		
CBT		2.629	730	279
FOBT		2.988	730	279
TE based and zig-zag models [37]				
$N = 1$	zz	2.992	730	279
		2.992	730	372
$N = 2$	zz	2.985	730	558
		2.986	730	651
$N = 3$	zz	3.032	729	930
		3.033	729	1023
$N = 9$	zz	3.039	661	5115
		3.040	661	5208
Multi-line model based on TE [42]				
ML		3.026	731	6696
LE models [44]				
8L9		3.029	730	4743
HLE models				
8HL1		3.053	731	1674
8HL2		3.073	730	3999
8HL3		3.075	730	6324
8HL4		3.087	730	9393
8HL5		3.091	729	13206
8HL6		3.094	726	17763
8HL7		3.100	725	23064
8HL8		3.104	723	29109

Table 4: Maximum deflection and longitudinal stress at mid span, σ_{yy}, of the eight-layers composite beam
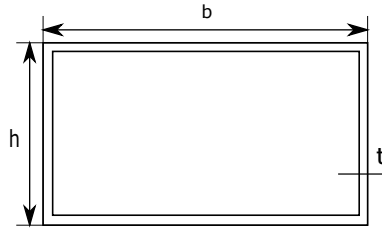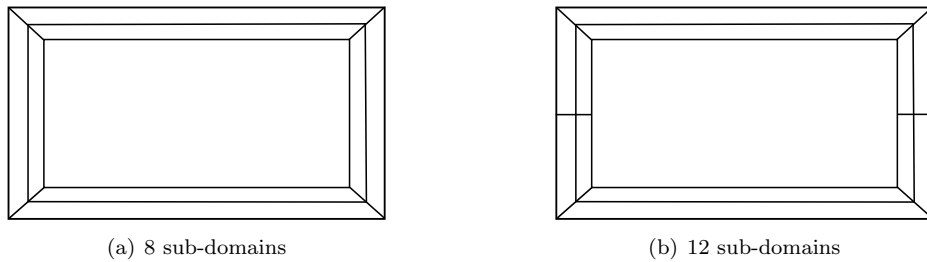

Figure 12: Box section geometry

(a) 8 sub-domains

(b) 12 sub-domains

Figure 13: Cross-section domain distributions

cross-sections, in which the capabilities of this type of local expansions can be better exploited. Figure 12 represents the cross-section geometry of the box beam studied for this assessment. The cross-section dimensions are: width, b, equal to 24.2 mm, height, h, equal to 13.6 mm and thickness, t, equal to 0.762 mm. Three different slenderness ratios, L/b, are considered: 10, 20 and 30. Each wall of the beam consists in a two-layer lamination: $[0°, 90°]$ for the flanges and $[-45°, 45°]$ for the webs, being the $0°$ and $-45°$ fiber-direction layers placed outwards. The mechanical characteristics of the orthotropic material used for the lamination are: $E_L = 69.0$ GPa, $E_T = E_z = 10.0$ GPa, $\nu_{LT} = \nu_{Lz} = \nu_{Tz} = 0.25$, $G_{LT} = G_{Lz} = G_{Tz} = 6$ GPa. Two domain configurations for HLE models are accounted for (see Fig. 13). The first one adopts a 12 sub-domain distribution above the cross-section, whereas the second one only uses 8 sub-domains. The beam is clamped at one edge and loaded with two vertical forces of 50 N each applied at the top corners of the tip.

The results of displacements and stresses are evaluated in the most determinant points of the beam. Classical models, LE and TE solutions (see Carrera *et al.* [44]) are included together with the solutions obtained with a MSC/Nastran solid model. Tables 5, 6 and 7 show the results for displacements and stresses for the different slenderness ratios considered. Out of these results, it is possible to state that:

- As expected, although classical models reach acceptable results for displacements in pure bending cases, they are not capable to deal with the calculation of the shear stresses, since by assumption they neglect some of the kinematic terms required for it.

- On the other hand, higher-order TE and LE models provide good results for both displacements and stresses with much lower computational costs than the 3D model. HLE models converge to the solid solution for low expansion orders even when the number of cross-section sub-domains is less than the LE model.

- An interesting fact can be observed regarding the 8HLE model (see Table 5), in which the flanges are modeled with just one sub-domain per layer. Less than 5% error in displacements and normal stresses for all expansion orders (but the first) has been obtained using this simplified cross-section configuration, proving the capability of this model of increasing the accuracy of the results through an enrichment of the kinematic field and not through a refinement of the cross-section layer domain. Although the values of the shear stresses of the 8HLE models are similar to those of the 12HLE models, they oscillate around the solid solution with slightly higher error rates. Again, this numerical issue could be solved by refining the longitudinal mesh, as explained in the convergence analysis of the first assessment (see Section 5.1).

Figure 14 (a) shows the normal stress distribution at the top flange along the z-axis at the middle section, whereas Fig. 14 (b) the distribution of shear stresses along the right exterior flange. Regarding the latter one, it is possible to appreciate how HLE models provide good results for the shear stresses even when employing just one element along the flange (8HL8 model). Finally, Figs. 15 and 16 show the normal and shear stresses of the two models considered, respectively, above the cross-section at mid span in a color-scaled plot.

5.5 Multi cell box beam

For the last assessment, a two-cell cantilever beam with a cut is considered. The section is forced to open at the cut placed in one of the cells. This configuration allows to test not only the bending capabilities, but

model	$-u_z \times 10^3$	$\sigma_{yy} \times 10^6$	$\sigma_{yy} \times 10^6$	$\sigma_{yz} \times 10^6$	$DOFs$
	[0,L,+h/2]	[0,L/2,+h/2]	[0,0,+h/2]	[b/2,L/2,+h/4]	
SOLID [44]	7.17	85.40	165.4	−8.93	360000
Classical and refined models based on TE [44]					
EBBM	7.09	85.24	170.48	0	155
TBM	7.15	85.27	170.51	−6.40	600
$N=3$	7.09	84.44	163.50	−9.64	930
$N=6$	7.16	85.30	165.77	−8.94	2604
LE models [44]					
16L9	7.16	85.80	167.74	−8.31	7740
HLE models					
12HL1	7.04	84.40	170.41	−8.13	1674
12HL2	7.19	85.35	166.75	−8.51	4464
12HL3	7.13	85.32	166.13	−9.32	7254
12HL4	7.17	85.21	165.77	−9.17	11160
12HL5	7.17	85.22	166.27	−8.15	16182
12HL6	7.17	85.37	166.55	−8.17	22320
12HL7	7.17	85.45	166.66	−8.92	29574
12HL8	7.24	85.33	166.53	−9.01	37944
8HL1	6.82	82.23	166.84	−13.12	1116
8HL2	7.15	85.02	173.20	−8.00	2976
8HL3	7.16	84.94	171.30	−7.92	4836
8HL4	7.18	85.18	166.45	−8.37	7440
8HL5	7.19	85.07	167.31	−9.53	10788
8HL6	7.19	84.92	171.89	−9.26	14880
8HL7	7.19	85.08	172.01	−8.61	19716
8HL8	7.20	85.32	168.80	−7.92	25296

Table 5: Displacements and stresses of the single-cell beam for both domain configurations (L/b=10)

model	$-u_z \times 10^3$	$\sigma_{yy} \times 10^6$	$\sigma_{yy} \times 10^6$	$\sigma_{yz} \times 10^6$	$DOFs$
	[0,L,+h/2]	[0,L/2,+h/2]	[0,0,+h/2]	[b/2,L/2,+h/4]	
SOLID [44]	56.80	170.90	338.10	−12.85	360000
Classical and refined models based on TE [44]					
EBBM	56.43	170.48	340.96	0	155
TBM	56.51	170.48	340.96	−10.30	600
$N=3$	55.86	169.19	331.75	−14.74	930
$N=6$	56.25	170.88	332.18	−13.66	2604
LE models [44]					
16L9	56.70	170.52	336.49	−12.11	7740
HLE models					
12HL1	55.98	168.21	336.04	−11.77	1674
12HL2	56.62	170.84	336.35	−13.05	4464
12HL3	56.68	170.98	336.22	−15.33	7254
12HL4	56.71	170.90	336.0	−14.94	11160
12HL5	56.74	170.91	336.68	−12.25	16182
12HL6	56.75	170.72	337.04	−12.43	22320
12HL7	56.76	170.81	337.31	−13.72	29574
12HL8	56.77	170.72	337.27	−13.80	37944

Table 6: Displacements and stresses of the single-cell beam for the 12HLE model (L/b=20)

model	$-u_z \times 10^3$	$\sigma_{yy} \times 10^6$ [0,L,+h/2]	$\sigma_{yy} \times 10^6$ [0,L/2,+h/2]	$\sigma_{yz} \times 10^6$ [0,0,+h/2]	$DOFs$ [b/2,L/2,+h/4]
SOLID [44]	191.28	256.37	509.14	-16.77	360000
Classical and refined models based on TE [44]					
EBBM	191.45	255.72	511.45	0	155
TBM	191.71	255.72	511.45	-14.21	600
$N = 3$	189.39	253.92	499.62	-19.66	930
$N = 6$	190.59	256.71	500.89	-18.36	2604
LE models [44]					
16L9	191.85	256.23	504.25	-15.63	7740
HLE models					
12HL1	188.73	252.57	502.52	-15.04	1674
12HL2	190.74	256.22	504.38	-17.63	4464
12HL3	190.89	256.57	504.50	-22.15	7254
12HL4	190.95	256.68	504.41	-21.86	11160
12HL5	191.05	256.67	505.18	-18.21	16182
12HL6	191.06	256.57	505.51	-18.22	22320
12HL7	191.11	256.71	505.87	-19.53	29574
12HL8	191.12	256.51	505.90	-19.54	37944

Table 7: Displacements and stresses of the single-cell beam for the 12HLE model (L/b=30)
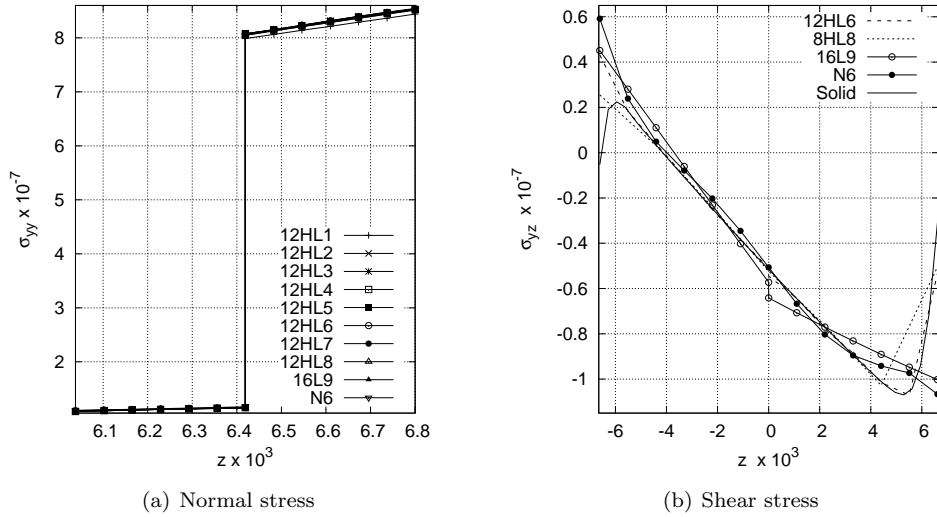

(a) Normal stress

(b) Shear stress

Figure 14: Normal stress distribution, σ_{yy}, along the thickness of the top flange (a) and shear stress distribution, σ_{yz}, along the inner layer of the right web (b) of the single-cell box beam ($L/b = 10$)
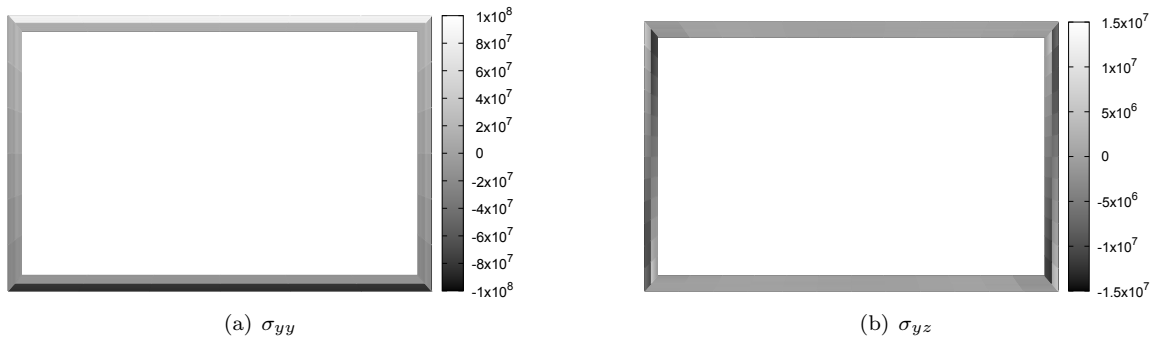

(a) σ_{yy}

(b) σ_{yz}

Figure 15: Normal and shear of the single-cell 8HL5 model

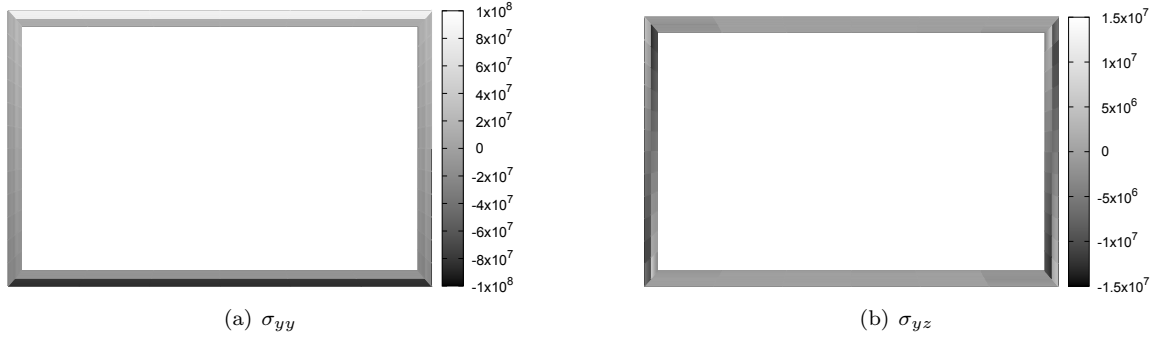(a) σ_{yy}

(b) σ_{yz}

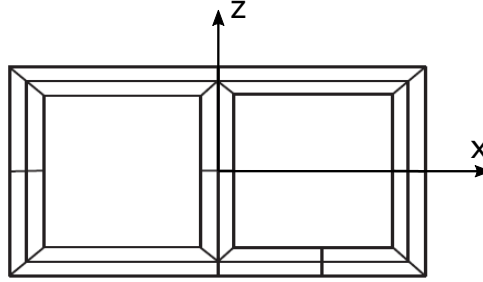Figure 16: Normal and shear of the single-cell 12HL5 model

Figure 17: Cross-section domain distribution of the two-cell beam

also the in-plane deformations at the cross-sectional level. The lamination and the dimensions are the same as the single-cell beam, but a third web is added in the middle of the section, dividing the central space in two equal cells. The cut is placed at the bottom of the right cell. As for the previous assessments, the LW approach has been conducted by using a 22 sub-domain configuration at cross-section level (see Fig. 17).

Two vertical and two horizontal point loads of 50 N each are applied at the tip section. The two vertical forces are directed upwards and they are located at the two corners of the top flange, whereas the two horizontal loads have opposite directions: the load applied at the bottom right corner is oriented to the positive direction of the x-axis, while the other one, applied and the bottom left corner, is directed towards the negative values of the x-axis. Figure 18 displays the deformed of the tip cross-section. HLE models are capable to capture both the bending curvature upwards along the y-axis caused by the vertical loads, and the in-plane opening of the right cell caused by the horizontal loads. Finally, both normal and shear stress section distributions at the mid span are displayed in Fig. 19.

6   Conclusions

The aim of the present work has been to introduce, test and validate a Hierarchical Legendre-type one-dimensional model applied to the analysis of composite structures. The model, developed in the framework of the Carrera Unified Formulation (CUF), have demonstrated to be a powerful tool for the analysis of composite structures. Many examples have been carried out in order to compare the results with others from the literature, including compact cross-ply laminates, thin-walled boxes and open beams. MSC/Nastran solid elements solutions have also been used as a reference due to its high accuracy in thin-walled cases. The Hierarchical Legendre Expansions (HLE) have shown their potential and liability. Out of these results, it is
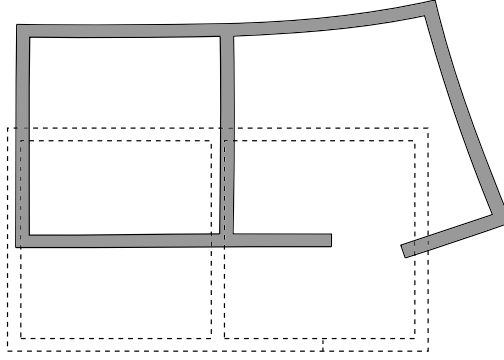
Figure 18: Deformed cross-section at the tip of the two-cell beam

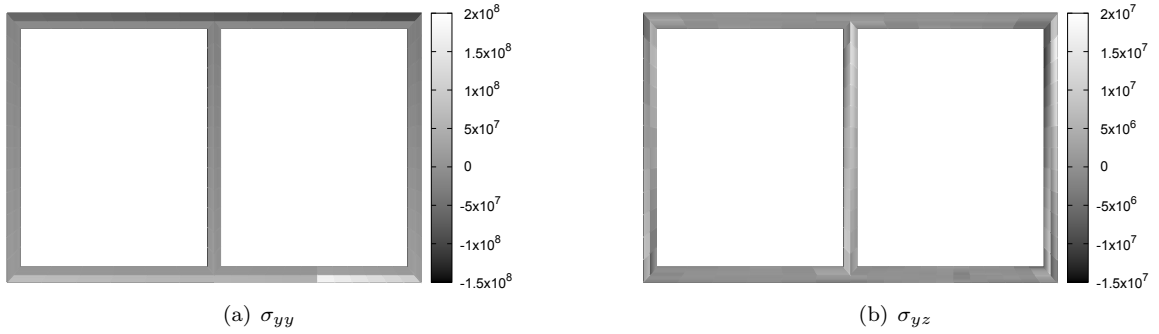(a) σ_{yy}

(b) σ_{yz}

Figure 19: Normal and shear stresses of the 22HL5 model at mid span

possible to state:

- HLE have demonstrated to be highly adequate to obtain Layer Wise models. While Lagrange-based CUF model requires the use of multi-domain layers to improve the theory kinematics, HLE variable kinematics allows to develop single-domain Layer Wise models, in which each layer is described by only one local expansion. The precision of the solutions can be tuned by just changing the polynomial order, which is, in fact, a free-parameter of the model.

- According to the results obtained in this work, the HLE have shown its advantages in the modelling of composite structures, representing accurately the local behaviour of the single layers while diminishing the number of expansion domains above the section in comparison with the other models taken as a reference.

This work set the basis of the HLE applications to the modelling of composite structures. Here, only straight geometries have been considered, but the variable kinematic order employed in this formulation can eventually be used to generate curved domains. This capability represents one of the main potentials of HLE and opens the path to further developments regarding the modelling of curved slender structures, such as fuselages and wings, and multi-scale fiber-matrix systems.

Acknowledgements

References

[1] S. W. Tsai. *Composites Design.* Dayton, Think Composites, 4th edition, 1988.

[2] L. Euler. *De curvis elasticis.* Lausanne and Geneva: Bousquet, 1744.

[3] S. P. Timoshenko. On the transverse vibrations of bars of uniform cross section. *Philosophical Magazine*, 43:125–131, 1922.

[4] E. Reissner and Y. Stavsky. Bending and stretching of certain types of heterogeneous aeolotropic elastic plates. *Journal of Applied Mechanics*, 28:402–408, 1961.

[5] E. Reissner. The effect of transverse shear deformation on the bending of elastic plates. *Journal of Applied Mechanics*, 12(2):69–77, 1945.

[6] R. Mindlin. Influence of rotary inertia and shear flexural motion of isotropic, elastic plates. *Journal of Applied Mechanics*, 18:31–38, 1951.

[7] R.K. Kapania and S. Raciti. Recent advances in analysis of laminated beams and plates, part I: Shear effects and buckling. *AIAA Journal*, 27(7):923–935, 1989.

[8] R.K. Kapania and S. Raciti. Recent advances in analysis of laminated beams and plates, part II: Vibrations and wave propagation. *AIAA Journal*, 27(7):935–946, 1989.

[9] J. N. Reddy. A simple higher-order theory for laminated composites. *Journal of Applied Mechanics*, 51:745–752, 1986.

[10] A. Khdeir and J. Reddy. Buckling of cross-ply laminate beams with arbitrary boundary conditions. *Composite Structures*, 37:1–3, 1997.

[11] A. Khdeir and J. Reddy. Buckling of cross-ply laminate beams with arbitrary boundary conditions. *Composite Structures*, 37:195–203, 1997.

[12] H. Matsunaga. Interlaminar stress analysis of laminated composite beams according to global higher-order deformation theories. *Composite Strucutures*, 55:105–114, 2002.

[13] H. Matsunaga. Vibration and buckling of multilayered composite beams according to higher order deformation theories. *Journal of Sound and Vibration*, 246(1):47–62, 2001.

[14] M.K. Rao, Y. Desai, and M. Chistnis. Free vibrations of laminated beams using mixed theory. *Composite Structures*, 52:149–160, 2001.

[15] M. Karama, K. Afaq, and S. Mistou. Mechanical behaviour of laminated composite beam by the new multi-layered laminated composite structures model with transverse shear stress continuity. *International Journal of Solids and Structures*, 40:1525–1546, 2003.

[16] P. Vidal, L. Gallimard, and O. Polit. Composite beam finite element based on the proper generalized decomposition. *Computers and Structures*, 102-103:76–86, 2012.

[17] P. Vidal and O. Polit. A sine finite element using a zig-zag function for the analysis of laminated composite beams. *Composites*, 43:1671–1682, 2011.

[18] N.J. Pagano. Exact solutions for composite laminates in cylindrical bending. *Journal of Composite Materials*, 3(3):398–411, 1969.

[19] R. P. Shimpi and Y. M. Ghugal. A new layerwise trigonometric shear deformation theory for two-layered cross-ply beams. *Composites Science and Technology*, 61(9):1271 – 1283, 2001.

[20] K. Surana and S. Nguyen. Two-dimensional curved beam element with higher-order hierarchical transverse approximation for laminated composites. *Computers and Structures*, 36:499–511, 1990.

[21] M. Tahani. Analysis of laminated composite beams using layerwise displacement theories. *Composite Structures*, 79(4):535 – 547, 2007.

[22] A. J. M. Ferreira. Analysis of composite plates using a layerwise theory and multiquadrics discretization. *Mechanics of Advanced Materials and Structures*, 12(2):99–112, 2005.

[23] W.J. Na and J.N. Reddy. Delamination in cross-ply laminated beams using the layerwise theory. *Asian Journal of Civil Engineering*, 10(4):451–480, 2009.

[24] Y.M. Ghugal and S.B. Shinde. Static flexure of cross-ply laminated cantilever beams. *Composites: Mechanics, Computations, Applications*, 5(3):219–243, 2014.

[25] J. N. Reddy. On refined computational models of composite laminates. *International Journal for Numerical Methods in Engineering*, 27(2):361–382, 1989.

[26] R.P. Shimpi and A.V. Ainapure. A beam finite element based on layerwise trigonometric shear deformation theory. *Composite Structures*, 53(2):153 – 162, 2001.

[27] L. Krger, A. Wetzel, R. Rolfes, and K. Rohwer. A three-layered sandwich element with improved transverse shear stiffness and stresses based on {FSDT}. *Computers and Structures*, 84(1314):843 – 854, 2006.

[28] D.H. Li, Y. Liu, and X. Zhang. An extended layerwise method for composite laminated beams with multiple delaminations and matrix cracks. *International Journal for Numerical Methods in Engineering*, 101(6):407–434, 2015.

[29] E. Carrera, A. Pagani, M. Petrolo, and E. Zappino. Recent developments on refined theories for beams with applications. *Mechanical Engineering Reviews*, 2(2):14–00298, 2015.

[30] E. Carrera. Theories and finite elements for multilayered, anisotropic, composite plates and shells. *Archives of Computational Methods in Engineering*, 9(2):87–140, 2002.

[31] E. Carrera. Theories and finite elements for multilayered plates and shells: a unified compact formulation with numerical assessment and benchmarking. *Archives of Computational Methods in Engineering*, 10(3):216–296, 2003.

[32] E. Carrera and G. Giunta. Refined beam theories based on Carrera's unified formulation. *International Journal of Applied Mechanics*, 2(1):117–143, 2010.

[33] E. Carrera, G. Giunta, P. Nali, and M. Petrolo. Refined beam elements with arbitrary cross-section geometries. *Computers and Structures*, 88(5–6):283–293, 2010.

[34] E. Carrera, M. Petrolo, and P. Nali. Unified formulation applied to free vibrations finite element analysis of beams with arbitrary section. *Shock and Vibrations*, 18(3):485–502, 2011.

[35] E. Carrera and M. Petrolo. Refined beam elements with only displacement variables and plate/shell capabilities. *Meccanica*, 47(3):537–556, 2012.

[36] E. Carrera and M. Petrolo. Refined one-dimensional formulations for laminated structure analysis. *AIAA Journal*, 50(1):176–189, 2012.

[37] E. Zappino E. Carrera, M. Filippi. Laminated beam analysis by polynomial, trigonometric, exponential and zig-zag theories. *European Journal of Mechanics A/Solids*, 2013. Published.

[38] E. Carrera, M. Maiarù, and M. Petrolo. Component-wise analysis of laminated anisotropic composites. *International Journal of Solids and Structures*, 49(13):1839 – 1851, 2012.

[39] E. Carrera, M. Filippi, and E. Zappino. Analysis of rotor dynamic by one-dimensional variable kinematic theories. *Journal of Engineering for Gas Turbines and Power*, 135:1–9, 2013.

[40] E. Carrera, M. Filippi, and E. Zappino. Free vibration analysis of rotating composite blades via carrera unified formulation. *Composite Structures*, 106:317–325, 2013.

[41] E. Carrera and M. Filippi. Variable kinematic one-dimensional finite elements for the analysis of rotors made of composite materials. *Journal of Engineering for Gas Turbines and Power*, 136(9):art. n. 092501, 2014.

[42] E. Carrera and A. Pagani. Multi-line enhanced beam model for the analysis of laminated composite structures. *Composites: Part B*, 57:112–119, 2014.

[43] A. Pagani, E. Carrera, M. Boscolo, and J.R. Banerjee. Refined dynamic stiffness elements applied to free vibration analysis of generally laminated composite beams with arbitrary boundary conditions. *Composite Structures*, 110:305–316, 2014.

[44] E. Carrera, M. Filippi, P.K. Mahato, and A. Pagani. Accurate static response of single- and multi-cell laminated box beams. *Composite Structures*, 136:372–383, 2016.

[45] M. Filippi, A. Pagani, M. Petrolo, G. Colonna, and E. Carrera. Static and free vibration analysis of laminated beams by refined theory based on chebyshev polynomials. *Composite Structures*, 132:1248–1259, 2015.

[46] B. Szabó, A. Dster, and E. Rank. *The p-Version of the Finite Element Method*. John Wiley and Sons, Ltd, 2004.

[47] M. Petrolo E. Carrera, G. Giunta. *Beam structures: classical and advanced theories.* John Wiley and Sons, 2011.

[48] E. Carrera and A. Pagani. Free vibration analysis of civil engineering structures by component-wise models. *Journal of Sound and Vibration*, 333(19):4597–4620, 2014.

[49] E. Carrera, A. Pagani, and M. Petrolo. Component-wise method applied to vibration of wing structures. *Journal of Applied Mechanics*, 80(4):art. no. 041012 1–15, 2013.

[50] B. Szabó and I. Babuka. *Finite Element Spaces*, pages 145–165. John Wiley and Sons, Ltd, 2011.

[51] E. Carrera, A. Pagani, and M. Petrolo. Use of lagrange multipliers to combine 1d variable kinematic finite elements. *Computers and Structures*, 129:194–206, 2013.

[52] T.P. Vo and H.T. Thai. Static behavior of composite beams using various refined shear deformation theories. *Composite Structures*, 94:2513–2522, 2012.

[53] N.J. Pagano. Exact solutions for rectangular bidirectional composites and sandwich plates. *Journal of Composite Materials*, 4:20–34, 1970.

[54] G.M. Kulikov and R.S. Plotnikova. Solution of three-dimensional problems for thick elastic shells by the method of reference surfaces. *Mechanics of Solids*, 49(4):403–412, 2014.

[55] J. Davalos, Y. Kim, and E. Barbero. Analysis of laminated beams with a layerwise constant shear theory. *Composite Structures*, 38:241–253, 1994.

[56] Y.Z. Xiaoshan Lin. A novel one-dimensional two-node shear-flexible layered composite beam element. *Finite Elements in Analysis and Design*, 47:676–682, 2011.

[57] S.G. Lekhniskii. Anisotropic plates. *Gordon and Branch*, 1968.

A   Material coefficients in the material coordinate system

$$C_{11} = \frac{E_1(1-\nu_{23}\nu_{32})}{\Delta} \quad C_{12} = \frac{E_1(\nu_{21}+\nu_{23}\nu_{31})}{\Delta} \quad C_{13} = \frac{E_1(\nu_{31}+\nu_{21}\nu_{32})}{\Delta}$$

$$C_{21} = \frac{E_2(\nu_{12}+\nu_{13}\nu_{32})}{\Delta} \quad C_{22} = \frac{E_2(1-\nu_{13}\nu_{31})}{\Delta} \quad C_{23} = \frac{E_2(\nu_{32}+\nu_{12}\nu_{31})}{\Delta}$$

$$C_{31} = \frac{E_3(\nu_{13}+\nu_{12}\nu_{23})}{\Delta} \quad C_{32} = \frac{E_3(\nu_{23}+\nu_{13}\nu_{21})}{\Delta} \quad C_{33} = \frac{E_3(1-\nu_{12}\nu_{21})}{\Delta}$$

$$C_{44} = G_{21} \qquad\qquad C_{55} = G_{31} \qquad\qquad C_{66} = G_{23}$$

(33)

where

$$\Delta = 1 - \nu_{12}\nu_{21} - \nu_{12}\nu_{21} - \nu_{12}\nu_{21} - \nu_{12}\nu_{21}\nu_{31} - \nu_{12}\nu_{21}\nu_{31} \tag{34}$$

being the engineering modulus defined as

$$E_i = \frac{\sigma_i}{\varepsilon_i} \quad G_{ij} = \frac{\sigma_{ij}}{\varepsilon_{ij}} \quad \nu_{ij} = -\frac{\varepsilon_j}{\varepsilon_i} \tag{35}$$

B   Stiffness matrix integrals

The integrals of the transverse expansions above the cross-section surface, E, are defined as:

$$E_{\tau,x s,x} = \int_\Omega F_{\tau,x} F_{s,x}\, d\Omega, \quad E_{\tau,z s,z} = \int_\Omega F_{\tau,z} F_{s,z}\, d\Omega, \quad E_s^\tau = \int_\Omega F_\tau F_s\, d\Omega,$$

$$E_{\tau,x s,z} = \int_\Omega F_{\tau,x} F_{s,z}\, d\Omega, \quad E_{\tau,z s,x} = \int_\Omega F_{\tau,z} F_{s,x}\, d\Omega, \quad E_{\tau,x s} = \int_\Omega F_{\tau,x} F_s\, d\Omega,$$

$$E_{\tau s,x} = \int_\Omega F_\tau F_{s,x}\, d\Omega, \quad E_{\tau,z s} = \int_\Omega F_{\tau,z} F_s\, d\Omega, \quad E_{\tau s,z} = \int_\Omega F_\tau F_{s,z}\, d\Omega,$$

(36)

and the expressions I_{ij}, $I_{ij,y}$, $I_{i,y j}$, and $I_{i,y j,y}$ of the integrals of the shape functions along the physical coordinate y are:

$$I_{ij} = \int_l N_i N_j\, dy \qquad I_{ij,y} = \int_l N_i N_{j,y}\, dy$$

$$I_{i,y j} = \int_l N_{i,y} N_j\, dy \quad I_{i,y j,y} = \int_l N_{i,y} N_{j,y}\, dy$$

(37)